HHS Public Access

Author manuscript

Biomaterials. Author manuscript; available in PMC 2021 May 01.

Targeted Melanoma Radiotherapy Using Ultrasmall ^{177}Lu-Labeled α-Melanocyte Stimulating Hormone-Functionalized Core-Shell Silica Nanoparticles

Xiuli Zhang[a,b,1], **Feng Chen**[c,1], **Melik Z. Turker**[d], **Kai Ma**[e], **Pat Zanzonico**[f], **Fabio Gallazzi**[g], **Manankumar A. Shah**[a,b], **Austin R. Prater**[a,b], **Ulrich Wiesner**[d], **Michelle S. Bradbury**[c,h], **Michael R. McDevitt**[c], **Thomas P. Quinn**[a,b,*]

[a]Harry S. Truman Veterans' Hospital, 800 Hospital Dr., Columbia, MO 65201 United States

[b]Department of Biochemistry, University of Missouri, Columbia, Missouri 65211, United States

[c]Department of Radiology, Sloan Kettering Institute for Cancer Research, New York, New York 10065, United States

[d]Department of Materials Science and Engineering, Cornell University, Ithaca, New York 14853, United States

[e]Elucida Oncology, New York, NY 10016 United States

[f]Department of Medical Physics, Sloan Kettering Institute for Cancer Research, New York, New York 10065, United States

[g]Department of Chemistry and Research Core Facilities, University of Missouri, Columbia, Missouri 65211, United States

[h]Molecular Pharmacology Program, Sloan Kettering Institute for Cancer Research, New York, NY 10065, United States

[*]Corresponding author. Thomas P. Quinn, Biochemistry Department, 117 Schweitzer Hall, University of Missouri, Columbia, MO 65211 USA, Quinnt@missouri.edu, *Tel:* +1-573-882-6099, *Fax:* +1-573-882-5635.

Data Availability
Data will be made available on request.

Appendix A. Supplementary data
Supplementary data to this article can be found online.

Declaration of interests
The authors declare that they have no known competing financial interests or personal relationships that could have appeared to influence the work reported in this paper.

Competing financial interests
M.S.B. and U.W. hold interest in Elucida Technologies, Inc., which has licensed IP from Cornell and MSKCC on C' dots and their application in oncology.

Abstract

Lutetium-177 (^{177}Lu) radiolabeled ultrasmall (~6 nm dia.) fluorescent core-shell silica nanoparticles (Cornell prime dots or C' dots) were developed for improving efficacy of targeted radiotherapy in melanoma models. PEGylated C' dots were surface engineered to display 10–15 alpha melanocyte stimulating hormone (αMSH) cyclic peptide analogs for targeting the melanocortin-1 receptor (MC1-R) over-expressed on melanoma tumor cells. The ^{177}Lu-DOTA-αMSH-PEG-C' dot product was radiochemically stable, biologically active, and exhibited high affinity cellular binding properties and internalization. Selective tumor uptake and favorable biodistribution properties were also demonstrated, in addition to bulk renal clearance, in syngeneic B16F10 and human M21 xenografted models. Prolonged survival was observed in the treated cohorts relative to controls. Dosimetric analysis showed no excessively high absorbed dose among normal organs. Correlative histopathology of *ex vivo* treated tumor specimens revealed expected necrotic changes; no acute pathologic findings were noted in the liver or kidneys. Collectively, these results demonstrated that ^{177}Lu-DOTA-αMSH-PEG-C' dot targeted melanoma therapy overcame the unfavorable biological properties and dose-limiting toxicities associated with existing mono-molecular treatments. The unique and tunable surface chemistries of this targeted ultrasmall radiotherapeutic, coupled with its favorable pharmacokinetic properties, substantially improved treatment efficacy and demonstrated a clear survival benefit in melanoma models, which supports its further clinical translation.

Graphical Abstract
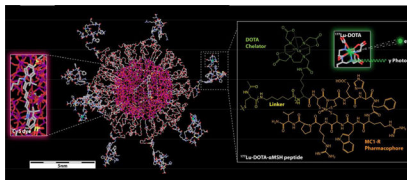
Keywords

ultrasmall silica nanoparticle; α-melanocyte stimulating hormone; melanoma; radionuclide therapy

1. Introduction

Revolutionary advances in metastatic melanoma treatment have been made over the past decade with targeted mutant B-Raf and MEK receptor tyrosine kinase (RTK) inhibitors and by checkpoint blockade immunotherapies [1–3]. Rapid and systemic elimination of tumors is often observed in patients treated with RTK inhibitors, however most patients relapse with lethal drug-resistant disease [4–5]. While systemic checkpoint blockade immunotherapy with cytotoxic T-lymphocyte antigen 4 (CTLA-4) and programmed cell death-1 (PD-1) antibodies has led to dramatic therapeutic responses, progression-free survival for combination immunotherapy has only been about 11.5 months [6]. Initial stereotactic radiotherapy plus combination immunotherapy studies have shown striking results in a subset of patients, fostering new clinical trials. [7]. Melanoma radiotherapy alone has

resulted in the shrinkage of distant tumors through the abscopal effect in a limited number of patients, and its immunological correlate has shown dramatic results in several case reports [8]. Despite exciting clinical results, immunotherapy side effects categorized as immune-related adverse events can lead to reduced efficacy or, in some instances, life-threatening conditions. Although there is considerable excitement around the application of immunotherapy and combination immunotherapy regimens to the treatment of metastatic melanoma, new synergistic therapeutic options are critically needed to simultaneously block multiple pathways controlling cancer cell proliferation.

Targeted radionuclide therapy for the systemic treatment of metastatic melanoma is an important clinical advance in the adjuvant setting. Preclinical studies, as well as several clinical trials, have demonstrated efficacy of small molecule, peptide and antibody targeting radiotherapies for treating melanoma [9]. Melanin targeting benzamides and antibodies have shown therapeutic efficacy in preclinical models and in limited clinical trials [10–11], while novel melanin targeting peptides have shown tumor growth control in melanoma-bearing mice [12]. Melanocortin-1 receptor (MC1-R) targeting alpha-melanocyte stimulating hormone (αMSH) peptides, radiolabeled with alpha- and beta-emitting radionuclides, have shown effective growth control of melanoma or its elimination in murine melanoma models [13–15]. In addition, the very late antigen-*4* (VLA-4) integrin-targeting peptides are promising for melanoma-targeted therapy [16–17]. However, dose-limiting toxicity has undermined clinical translation of these radionuclide therapies at doses necessary to achieve tumor eradication. Off-target accumulation in pigmented eyes with radiolabeled melanin-targeting therapeutics can limit administered activities, while extended circulation times for radiolabeled antibodies increases the risk of marrow toxicity [10, 12]. Moreover, non-specific renal uptake of radiolabeled peptides may impose an upper limit on administered therapeutic activities [18]. In addition, normal integrin expression in spleen and bone may be dose-limiting for cognate radioligands [16]. In summary, although studies to date highlight the effectiveness of targeted radiotherapies for treating melanoma, it will be crucial to demonstrate favorable pharmacokinetic (PK) and clearance profiles – without accompanying dose-limiting toxicity – for successful clinical translation.

Ultrasmall fluorescent core-shell silica nanoparticles, referred to as Cornell prime dots (C' dots), are silica core polyethylene glycol (PEG) shell nanoparticles (< 8 nm dia.) that have the potential to effectively deliver therapeutic radionuclides to sites of melanoma while overcoming many of the dose-limiting toxicities associated with current molecular therapeutics [19–22]. The PK and clearance properties of C' dots are situated between those of antibodies and peptides [21, 23]. Radiolabeled C' dots exhibit favorable clearance from the blood, and are primarily excreted through the kidneys, ultimately reducing the potential for marrow, liver, and/or colonic mucosal toxicity by limiting circulation times and largely avoiding hepatobiliary clearance [24]. Uptake of radiolabeled C' dots in liver and other reticuloendothelial system (RES) tissues is low, as is kidney uptake [25]. This property is critically important, given the radiosensitivity of the kidneys. In addition, this overcomes dose-limiting toxicities associated with the high non-specific renal uptake of radiometal-labeled peptides and antibody fragments. Phase 1, first-in-human imaging studies with integrin targeting [124]I-cRGDY–PEG–C dots previously demonstrated that the particle tracer was non-toxic and localized at sites of disease [26]. αMSH-bearing C' dots, or αMSH-PEG-

C' dots, which target a key melanoma biomarker, MC1-R, have been synthesized and radiolabeled for imaging [27]. Radio-iodinated and ^{89}Zr radiolabeled αMSH-PEG-C' dots were found to exhibit receptor-mediated uptake, along with favorable PK and target-to-background ratios [27].

In this study we report, for the first time, on the therapeutic efficacy of complexing agent 1,4,7,10-tetraazacyclododecane-1,4,7,10-tetraacetic acid (DOTA) functionalized αMSH-PEG-C' dots, or DOTA-αMSH-PEG-Cy5-C' dots, radiolabeled with the β-emitting radionuclide ^{177}Lu ($E_{\beta max}$ 0.497 MeV; $t_{1/2}$=6.65 days) in syngeneic and xenografted melanoma models (Fig. 1). To that end, ultrasmall PEGylated C' dots, covalently encapsulating the near infra-red (NIR) emitting dye Cy5, were engineered to display MC1-R targeting cyclic DOTA-αMSH peptides on their surfaces, according to published procedures [27]. The DOTA-αMSH-PEG-Cy5-C' dots contained an average of 1.6 dyes and 12.1 DOTA-αMSH peptides per nanoparticle. DOTA-αMSH-PEG-Cy5-C' dots were directly radiolabeled with ^{177}Lu, and assessed for active cell binding and favorable biodistribution profiles in B16F10 syngeneic and M21 xenograft models. Radiolabeled nanoparticles were radiochemically stable and rapidly internalized in B16F10 and M21 melanoma cells. Biodistribution studies revealed a relatively rapid clearance of radioactivity from the circulation, coupled with bulk renal excretion. Substantial tumor uptake was observed over the first 24 h. Single-photon emission tomography (SPECT) imaging with ^{177}Lu-DOTA-αMSH-PEG-Cy5-C' dots showed tumor uptake in M21 melanoma-bearing mice that could be blocked with excess non-radiolabeled DOTA-αMSH-PEG-Cy5-C' dots, suggesting specificity. Therapy studies showed that 177Lu-DOTA-αMSH-PEG-Cy5-C' dot treatment of B16F10 and M21 melanoma-bearing mice delayed tumor growth and increased median survival. These results support continued development of ^{177}Lu-DOTA-αMSH-PEG-Cy5-C' dots for melanoma radiotherapy.

2. Materials and methods

2.1. MC1-R targeting DOTA-αMSH peptide synthesis

The MC1-R targeting rhenium (Re) cyclized peptide DOTA-αMSH [Ac-Cys-(Ahx)$_2$-dLys(DOTA)-Re(Cys-Cys-Glu-His-dPhe-Arg-Trp-Cys)-Arg-Pro-Val-CONH$_2$] was synthesized using standard fluorenylmethyloxycarbonyl (Fmoc) solid-phase peptide synthesis (SPPS) chemistry on a Tetras peptide synthesizer (Advanced ChemTech). The peptides were purified using semi-preparative mass spectrometry (MS; LCQ-Fleet, Thermo-Fisher Scientific) guided high-performance liquid chromatography (HPLC).

2.2. DOTA-αMSH-PEG-Cy5-C' dot synthesis

The synthesis of DOTA-αMSH-PEG-Cy5-C' dot particles was based on procedures previously described [20, 27–28]. The resulting DOTA- α MSH-PEG-Cy5-C' dots were dialyzed against deionized water, purified using gel permeation chromatography (GPC), and filtered by sterile syringe filters. The final product was characterized and stored at 4°C [29–30].

2.3. Cell culture

B16F10 murine melanoma cells were obtained from American Type Culture Collection (ATCC). The M21 human melanoma cell line was obtained from D. A. Cheresh (University of California San Diego). The cell lines were cultured in RPMI 1640 supplemented with 10% fetal calf serum, 2 mM L-glutamine and Penicillin Streptomycin.

2.4. DOTA-αMSH-PEG-Cy5-C' dot IC_{50} assays

The concentration of DOTA-αMSH peptide and DOTA-αMSH-PEG-Cy5-C' dots needed to inhibit 50% binding of a MC1-R standard radioligand was determined with B16F10 murine melanoma cells [27]. A competitive binding assay was performed with DOTA-αMSH and DOTA-αMSH-PEG-Cy5-C' dots with ^{125}I-NDP over a concentration range of 10^{-13} to 10^{-5} M using B16F10 melanoma cells. The IC_{50} values for DOTA-αMSH and DOTA-αMSH-PEG-Cy5-C' dots were calculated using GraphPad Prism V 7.03.

2.5. DOTA-αMSH-PEG-Cy5-C' dot confocal imaging studies

B16-F10 and M21 cells were incubated with DOTA-αMSH-PEG-C' dots (1.5 μM) for 4 hours, while Lysotracker Green (100 nM; Invitrogen) and Hoechst 33342 (10 μg/mL; Life Technologies) were added 30 minutes and 5 min prior to imaging. A Leica SP8 WLL confocal microscope (Leica Microsystems, Inc.) equipped with 405 nm and tunable white light lasers, and a 40x/1.1NA water immersion objective was used for imaging. The excitation/emission band-path wavelengths used to detect Hoechst 33342, LysoTracker Green, and DOTA-αMSH-PEG-Cy5-C' dots were set to 405/430–480, 488/500–550, and 650/655–725 nm, respectively. All images were deconvolved with Huygens Professional 19.04 software program (SVI, Netherlands).

2.6. ^{177}Lu-DOTA-αMSH-PEG-Cy5-C' dot labeling and stability

[177]Lu chloride was obtained from the University of Missouri Research Rector (MURR). For C' dot radiolabeling, ^{177}Lu in 50 μL of NH_4Ac buffer (pH 5.5) was added to a vial containing a 10× molar excess of 15 μM DOTA-αMSH-PEG-Cy5-C' dots. The pH of the labeling reaction was adjusted to 5.5 if needed prior to incubation at 70°C for 20 minutes. The labeling reaction was quenched by adding 10 μL of 0.2 M EDTA and incubated for another 1 h at 37°C prior to use. The radiochemical yield was determined by ITLC. ^{177}Lu-DOTA-αMSH-PEG-Cy5-C' dot stability was determined by incubating 100 μL of the ^{177}Lu-DOTA-αMSH-PEG-Cy5-C' dot solution with 100 μL of water, phosphate buffered saline (PBS), mouse serum or human serum at 37°C for 1 h, 4 h, and 24 h then assayed by instant thin layer chromatography (ITLC).

2.7. Cellular binding and internalization of ^{177}Lu-DOTA-αMSH-PEG-Cy5-C' dots

B16F10 murine melanoma cells, M21 human melanoma cells, human embryo kidney-293 (HEK293) cells, retinal epithelia cells (ARPE-19), and normal prostate epithelial cells (RWPE-1) were plated in a 24 well plates (0.2 million/well) and grown overnight at 37°C. Approximately, 100,000 CPM of ^{177}Lu-DOTA-αMSH-PEG-Cy5-C' dots were added to each well for cell binding studies at 25°C. For specificity studies, 100,000 CPM of ^{177}Lu-DOTA-αMSH-PEG-Cy5-C' dots or ^{177}Lu-DOTA-αMSH-PEG-Cy5-C' dots + 5 μg of NDP

peptide were added to each well. At 6 h, 18 h and 24 h post-incubation, the cells were rinsed and surface-bound radioactivity was obtained with an acidic buffer wash (40 mM sodium acetate pH 4.5, 0.9% NaCl and 0.02% BSA). Internalized activity was obtained by lysing cells with 1 M NaOH after the acid buffer wash. Quantitation of radioactivity in the membrane-bound and the internalized fractions was performed with a γ-counter.

2.8. ^{177}Lu-DOTA-αMSH-PEG-Cy5-C' dot biodistribution studies

Animal studies were conducted in compliance with Institutional Animal Care and Use Committee rules for animal experimentation at the University of Missouri, Harry Truman Veterans' Hospital and Memorial Sloan Kettering Cancer Center. Female and male C57 and nude mice were inoculated subcutaneously in the flank or shoulder with 1 million cultured B16/F10 murine melanoma cells or 10 million M21 human melanoma cells (2:1 PBS:matrigel), respectively. For biodistribution studies, a 5 µCi solution of ^{177}Lu-DOTA-αMSH-PEG-Cy5-C' dots were injected into the tail veins of B16F10 (n=4) and M21 (n=3) tumor-bearing mice when tumors reached 0.5 g. At prescribed p.i. time points, mice were sacrificed and major organs and tissues removed, weighed, and radioactivity quantitated using a γ-counter. Data were calculated as a percentage of the injected dose (% ID) or percentage of the injected dose per gram (% ID/g) of tissue, plus or minus the standard deviation (± s.d.).

2.9. Imaging studies

SPECT imaging studies were performed in M21 tumor-bearing SCID mice injected with 800 µCi ^{177}Lu-DOTA-αMSH-PEG-Cy5-C' dots or ^{177}Lu-DOTA-αMSH-PEG-Cy5-C' dots + 200 µg NDP peptide. Imaging was conducted 24 h p.i. on a Siemens Inveon SPECT/CT small animal imaging system (Siemens Medical Solutions).

2.10. Dosimetry

Organ time-activity data were fit to exponential functions and analytically integrated, incorporating the effect of the radioactive decay of the ^{177}Lu, to derive the time-integrated activities. The mouse organ time-integrated activities were scaled by mouse-to-man total-body mass ratios to yield the organ time-integrated activities for the 70-kg Reference Adult. The Reference Adult mean normal absorbed doses were then calculated using the OLINDA computer program [31]. The mean mouse tumor absorbed doses were calculated using the tumor time-activity data and time-integrated activities and assuming complete local absorption of the ^{177}Lu beta particles and ignoring the small contribution of the ^{177}Lu gamma rays.

2.11. Therapy studies

Mice were inoculated with B16F10 or M21 melanoma cells in their flanks, as described in the biodistribution section. Therapy studies began when M21 and B16F10 tumors reached 0.01 cm^3 and 0.005 cm^3, respectively. Groups of M21 mice ($n = 8$) were i.v.-injected with 1 mCi and 0.5 mCi of ^{177}Lu-DOTA-αMSH-PEG-Cy5-C' dots, 1 mCi and 0.5 mCi (n=4) of ^{177}Lu-DOTA-PEG-Cy5-C' dots, DOTA-αMSH-PEG-Cy5-C' dots, or PBS control. Groups of B16F10 mice ($n = 10$) were also injected with 0.5 mCi of ^{177}Lu-DOTA-αMSH-PEG-

Cy5-C' dots, 0.5 mCi of ^{177}Lu-DOTA-PEG-Cy5-C' dots, DOTA-αMSH-PEG-Cy5-C' dots, or PBS control. All mice were monitored twice weekly for tumor size, weight, and body score index. Tumor volumes were calculated by caliper measurements of their length, width, and depth. Mice were removed from the study and sacrificed if body weight loss was >15% of the initial weight, tumor size exceeded 1.0 cm^3, a body score index of < 2 (0–5 scale), the appearance of skin ulcerations at the tumor site, or abnormal behaviors.

2.12. Statiatical analysis

IC$_{50}$ calculations were performed using Prism (Graphpad, Inc.) using non-linear regression data analysis and 95% confidence intervals. Therapy study survival curve evaluation and graph generation were performed using Prism-7 and Kaplan-Meier analysis [32]. Statistical comparisons between experimental groups were performed by Student's t-test (unpaired, two-tailed) or Gehan-Breslow-Wilcoxon test depending on the analysis [33]. Statistical significance for all tests was set at p<0.05.

3. Results and discussion

3.1. MC1-R targeting peptide and DOTA-αMSH-PEG-Cy5-C' dot synthesis

The MC1-R targeting DOTA-αMSH cyclic peptide [Ac-Cys-(Ahx)$_2$-dLys(DOTA)-Re(Cys^3-Cys^4-Glu^5-His^6-dPhe^7-Arg^8-Trp^9-Cys^{10})-Arg^{11}-Pro^{12}-Val^{13}-NH$_2$] used in C' dot synthesis was produced by solid phase peptide synthesis using standard Fmoc chemistry. Linear DOTA-αMSH peptide was cyclized on resin via rhenium (Re) coordination between three orthogonally deprotected cysteine residues (Cys^{3,4,10}) flanking the receptor binding region (Fig. S1a). The peptide was deprotected and cleaved from the resin. Crude peptide was purified to homogeneity using liquid chromatography-mass spectrometry (LC-MS) guided high-performance liquid chromatography (HPLC) purification (Fig. S1b). Analytical LC-MS analysis confirmed the final product had the expect mass (Fig. S1c). DOTA was selected as the radiometal chelator due to its ability to stably coordinate a number of therapeutic radionuclides, including ^{177}Lu. The dual 6-amino hexanoic acid (Ahx)$_2$ linker was employed to separate the receptor binding pharmacophore from the amino-terminal Ac-Cys nanoparticle attachment site.

Cyclic DOTA-αMSH peptide-bearing C' dots were prepared using a water-based synthesis protocol described previously, yielding ultrasmall (~6 nm dia.) silica nanoparticles (Fig. 1) [20, 27–28]. In short, during the synthetic process silane-modified Cy5 dye molecules were added to the silica sol-gel reaction forming the fluorescent silica core. DOTA-αMSH peptides were conjugated to maleimide-PEG-silane obtained from reaction of heterobifunctional maleimide-PEG-N-hydroxysuccinimide ester (mal-PEG-NHS) with aminopropyl-silane. The conjugate was then added together with regular PEG-silane to form the PEG shell of the silica nanoparticle. The resulting DOTA-αMSH-PEG-Cy5-C' dots were purified by gel permeation chromatography (GPC, Fig. 2a). A representative TEM of the GPC purified DOTA-αMSH-PEG-Cy5-C' dots, demonstrated uniform morphology, is shown in the Fig. 2a-insert. The average hydrodynamic diameter of the DOTA-αMSH-PEG-Cy5-C' dots was 5.8 nm as determined by fluorescence-correlation spectroscopy (FCS, Fig. 2b). FCS curve fits were also used to determine the concentration of the DOTA-αMSH-

PEG-Cy5-C' dot particles [29–30]. Optical (UV-Vis) spectroscopy was employed together with FCS determined concentration information to determine the average number of DOTA-αMSH peptides and Cy5 dye molecules per particle (Fig. 2c–e) [34]. To determine the average number of peptides per particle a calibration using absorbance at 256 nm ($\varepsilon = 8320$ M^{-1}, cm^{-1}) was employed (Fig. 2c–d). Absorbance contributions to the DOTA-αMSH-PEG-Cy5-C' dot spectra by DOTA-αMSH and Cy5 components, as revealed by a deconvolution method described earlier, are shown in Fig. 2e [34]. This spectral analysis determined that there were, on average, 12.1 DOTA-αMSH peptides and 1.6 Cy5 dyes per particle.

3.2. DOTA-αMSH-PEG-Cy5-C' in vitro receptor binding, uptake and affinity

A competitive binding assay, using the very high affinity MC1-R agonist ^{125}I-NDP [^{125}I-(Nle[4], D-Phe[7])-αMSH], [35] was performed to determine the IC_{50} for binding of DOTA-αMSH-PEG-Cy5-C' dots to MC1-R-expressing B16F10 melanoma cells (Fig. 2f). An IC_{50} value of 4.1×10^{-10} M was determined for the DOTA-αMSH-PEG-Cy5-C' dots, which was approximately 10× lower than the DOTA-αMSH peptide (3.3×10^{-9} M); this result highlights an increased affinity due to a multi-dentate peptide display on the C' dot surface. The IC_{50} value for the DOTA-αMSH-PEG-C' dots was comparable to that of αMSH-PEG-Cy5-C' dots (6.6×10^{-10} M), demonstrating that addition of the DOTA chelator did not adversely affect MC1-R binding [27].

Internalization of DOTA-αMSH-PEG-Cy5-C' dots in M21 and B16F10 melanoma cells was visualized by confocal microscopy (Fig. 3a). The Cy5-encapsulating silica core allowed direct detection of C' dots within live cells 4 h after addition to the culture media. The DOTA-αMSH-PEG-Cy5-C' dots were visualized within the cytoplasm of the melanoma cells (Fig. 3a(i)). Acidic cytoplasmic vesicles, such as lysosomal vesicles, were visualized using LysoTracker Green (Fig. 3a(ii)). Cellular nuclei were visualized by Hoechst fluorescent staining (Fig. 3a(iii)). Merged images of all three probes demonstrated that the DOTA-αMSH-PEG-Cy5-C' dots colocalized with the LysoTracker Green dye in the cytoplasm (Fig. 3a(iv)). These results showed that the majority of the internalized DOTA-αMSH-PEG-Cy5-C' dots were located in cytoplasmic acidic vesicles of both cell types, such as lysosomes, which is consistent with receptor-mediated particle endocytosis.

3.3. ^{177}Lu-DOTA-αMSH- PEG-Cy5-C' dot radiolabeling and cell binding

DOTA-αMSH-PEG-Cy5-C' dots were radiolabeled in 0.2 M NH_4OAc at pH 5.5 with $^{177}LuCl_3$ at 70°C for 20 min. The molar ratio of DOTA-αMSH-PEG-Cy5-C' dots to $^{177}LuCl_3$ was 10:1. The reaction was quenched by the addition of EDTA (0.01M) and subsequent incubation at 37°C for 60 min. Radiochemical yields were typically >95%. Any remaining free $^{177}LuCl_3$ was removed by PD-10 (Sephadex G-25) desalting columns yielding a final ^{177}Lu-DOTA-αMSH-PEG-Cy5-C' dot specific activity of 5.5×10^6 Ci/mol. The radiochemical stability of ^{177}Lu-DOTA-αMSH-PEG-Cy5-C' dots remained at >90% over a 24 h period at 37°C in normal saline and mouse serum (Table S1). *In vitro* cell binding studies were performed with ^{177}Lu-DOTA-αMSH-PEG-Cy5-C' dots using B16F10 and M21 melanoma cells (Fig. 3b). ^{177}Lu-DOTA-αMSH-PEG-Cy5-C' dots were bound and internalized by both the B16F10 and M21 melanoma cells. Membrane bound ^{177}Lu-DOTA-

αMSH-PEG-Cy5-C' dots were efficiently internalized over time. Cellular uptake could be blocked to background membrane bound levels using excess (5 μg) MC1-R-avid NDP peptide demonstrating MC1-R specificity of internalization. Cellular binding and internalization of ^{177}Lu-DOTA-αMSHPEG-Cy5-C' dots were examined in human embryonic kidney (HEK293) cells, human eye epithelial cells (ARPE-19) and normal prostate (RWPE-1) cells that do not express the MC1-R (Fig. S2). Uptake of ^{177}Lu-DOTA-αMSH-PEG-C' dots in normal MC1-R negative cells were below the amount of radioactivity found in the receptor-blocked samples in Fig. 3b. These results showed no significant normal cell line uptake of ^{177}Lu-DOTA-αMSH-PEG-C' dots, which is consistent with the biodistribution data.

Published reports specify the MC1-R densities of M21 and B16F10 cell lines as 1,281 receptors/cell and 2,884 receptors/cell, respectively [36–37]. The difference in MC1-R numbers per cell did not significantly affect cellular uptake of ^{177}Lu-DOTA-αMSH-PEG-Cy5-C' dots, underscoring the fact that a 2x difference in receptor numbers does not necessarily lead to a meaningful difference in internalized radioactivity. This is likely due to a lower specific activity of the ^{177}Lu-DOTA-αMSH-PEG-Cy5-C' dot preparation, which masks the difference in MC1-R numbers at early time points, but is evident at later time points. Both cell lines are in the median range for human melanoma MC1-R expression levels, which range from 900 to 5,500 receptors per cell [38]. In spite of relatively low receptor numbers, first in human melanoma imaging studies with a lactam cyclized αMSH peptide have validated targeting the MC1-R [39]. In summary, *in vitro* studies confirmed MC1-R selective binding and internalization of ^{177}Lu-DOTA-αMSH-PEG-Cy5-C' dots, highlighting the efficient delivery of a particle-based radiotherapy to tumor cells.

3.4. ^{177}Lu-DOTA-αMSH-PEG-Cy5-C' dots biodistribution, imaging and dosimetry

The biodistribution and PK profiles of intravenously (i.v.)-injected ^{177}Lu-DOTA-αMSH-PEG-Cy5-C' dots into B16F10 and M21 tumor-bearing mice were determined over a period of 96 h (Fig. 4). The bolus of activity injected into the bloodstream steadily declined and was nearly undetectable by 96 h post-injection (p.i.). Organs with high blood perfusion initially showed high uptake at 4 h, which subsequently declined over the ensuing 24 h period. For example, cardiac uptake values in B16F10 mice were 10.2±2.82% ID/g at 4 h and 3.92±0.76% ID/g at 24 h, while those for lungs were 12.1±0.83% ID/g at 4 h and 4.86±1.38% ID/g at 24 h p.i. Activities at 24 h p.i. in the liver and spleen were also low, with values of 5.76±0.61% ID/g and 5.10±1.24% ID/g, respectively. The clearance kinetics of activity from the blood, heart, lungs, and RES organs were slightly slower in the M21 xenograft model than in the C57 B16F10 syngeneic model. Blood activity at 24 h p.i. was 17.6±1.28% ID/g, approximately two times higher than that in B16F10 C57 mice. Uptake values in the lungs, liver, and spleen were nearly 1.5 times higher in the M21 tumor-bearing mouse at 24 h. Renal excretion was the primary route of clearance, with approximately 40% of the dose excreted at 24 h p.i. and nearly 80% excreted at 96 h p.i., in both animal models. Renal uptake values at 4 h, 24 h and 96 h p.i., respectively, were 14.6±1.14% ID/g, 13.1±1.57% ID/g and 4.42±1.06% ID/g in M21 tumor-bearing mice and 14.2±1.18% ID/g, 15.9±2.08% ID/g and 13.2±2.90% ID/g in B16F10 tumor-bearing mice.

We also measured renal uptake at 2 h p.i. (5.27±1.18% ID/g) in the B16F10 model for comparison with the αMSH peptide analog ^{177}Lu-DOTA-Re(Arg^{11})CCMSH (Fig. S3a) [40]. Renal activities measured after injection of the ^{177}Lu-DOTA-Re(Arg^{11})CCMSH peptide were 17.9±2.47% ID/g, 19.1±2.38% ID/g and 13.8±3.72% ID/g at 2 h, 4 h and 24 h p.i., respectively [40]. Relative to the particle-based probe, radiolabeled peptides showed greater renal retention at the early time points. Retention of radioactivity in the kidneys was non-specific since activity levels did not change in the blocking studies (Fig. S3b–c). These results demonstrate how the unique surface chemistry of the ^{177}Lu-DOTA-αMSH-PEG-Cy5-C' dots has the potential to mitigate kidney exposure compared to radiolabeled peptide alone. However, the level of renal uptake of the ^{177}Lu-DOTA-αMSH-PEG-Cy5-C' dots was higher than that observed in prior biodistribution studies using ^{125}I and ^{89}Zr labeled αMSH-PEG-C' dots [27]. On the basis of previously published radiolabeling studies of the DOTARe(Arg^{11})CCMSH peptide [13, 41–43], it is likely that the unique ^{177}Lu-DOTA chelator solution coordination geometry and net charge could have contributed to the higher renal retention seen with ^{177}Lu-DOTA-αMSH-PEG-Cy5-C' dots.

Targeted tumor uptake of ^{177}Lu-DOTA-αMSH-PEG-Cy5-C' dots was evident in both animal models. In M21 xenografts, tumor uptakes were 5.47±2.50% ID/g and 9.29±4.74% ID/g at 4 h and 24 h p.i., respectively, while tumor uptake in the B16F10 model was 10.4±3.56% ID/g at 4 h and 9.56±1.57% ID/g at 24 h. The progressively higher tumor uptakes from 4 h to 24 h p.i. are consistent with specific localization of the ^{177}Lu-DOTA-αMSH-PEG-Cy5-C' dots in tumor. Tumor uptake was blocked by about 50% in both mouse models by co-injecting excess NDP peptide (Fig. 4a and Fig. 4b inserts), likewise suggesting that uptake was largely MC1-R mediated.

Tumor uptake and selective tumor blocking of ^{177}Lu-DOTA-αMSH-PEG-Cy5-C' dots were visualized in the M21 model. The 208 keV gamma emission from ^{177}Lu allowed SPECT imaging of ^{177}Lu-DOTA-αMSH-PEG-Cy5-C' dots *in vivo*. Mice were administered ^{177}Lu-DOTA-αMSH-PEG-Cy5-C' dots alone or in the presence of excess i.v.-injected NDP peptide, and imaged 24 h p.i. (Fig. 5). SPECT-CT imaging results showed tumor uptake of ^{177}Lu-DOTA-αMSH-PEG-Cy5-C' dots (Fig. 5a and Fig. 5b), which could be blocked by excess MC1-R selective NDP peptide (Fig. 5c and Fig. 5d). This imaging study underscored the MC1-R selective uptake *in vivo*. These findings further emphasize the complementary dual-modality imaging capabilities of ^{177}Lu-DOTA-αMSH-PEG-Cy5-C' dots achievable with this platform, that is, high resolution optical imaging (Fig. 3a) alongside whole-body quantitative SPECT-CT imaging.

Organ absorbed doses were derived for a 70-kg Reference Adult using the MIRD formalism and the mouse ^{177}Lu-DOTA-αMSH-PEG-Cy5-C' dot time-activity data (Table 1) [31]. Low doses were found for liver and spleen, which was notable considering that these organs are often sites for non-specific accumulation of nanoparticle probes. Absorbed doses to other radiosensitive tissues, such as the red marrow and intestinal wall, were also low. The kidneys received the highest dose of any non-tumor tissue. Since the ^{177}Lu-DOTA-αMSHPEG-Cy5-C' dots exhibit primary renal clearance, a higher dose to the kidneys was not unexpected, but within tolerable limits. However, dosimetry findings were not significantly different from

those found using standard radiopharmaceuticals, suggesting that ^{177}Lu-DOTA-αMSH-PEG-Cy5-C' dots are safe and a clinically-promising agent for translation.

3.5.   ^{177}Lu-DOTA-αMSH-PEG-Cy5-C' dots therapy studies

The therapeutic efficacy of 177Lu-DOTA-αMSH-PEG-Cy5-C' dot treatment was examined in M21 and B16F10 melanoma-bearing mice (Fig. 6) Initial treatment doses were determined by maximum tolerated dose (MTD) studies in each model system. Mice were injected with 0.4 mCi, 0.7 mCi and 1 mCi of ^{177}Lu-DOTA-αMSH-PEG-Cy5-C' dots. The mice were observed for changes in weight and behavior over a 7- or 14-day period. Changes in body weight are reported in Table S2. Athymic nude mice bearing M21 tumors were more sensitive to treatment than B16F10 tumor-bearing C57 mice. The MTD was determined to be 1 mCi dose, since it resulted in weight loss that exceeded 15% of the initial weight, and approached the weight criterion for removing an animal from the therapy study. M21 tumor-bearing mice were randomized according to tumor size into five cohorts of mice, each for treatment with: 1 mCi or 0.5 mCi of ^{177}Lu-DOTA-αMSH-PEG-Cy5-C' dots, 1.0 mCi or 0.5 mCi of non-targeted ^{177}Lu-DOTA-PEG-Cy5-C' dots, non-radioactive DOTA-αMSH-PEG-Cy5-C' dots, or PBS control. All mouse groups receiving radiolabeled C' dots showed reduced tumor growth during the first 18 days of the study compared with groups receiving non-radiolabeled DOTA-αMSH-PEG-Cy5-C' dots or PBS control (Fig. 6a). Kaplan-Meier survival analysis revealed median survival times of 27, 41, 33, 60, 58 and 43 days for PBS control, DOTA-αMSH-PEG-Cy5-C' dots, ^{177}Lu-DOTA-PEG-Cy5-C' dots (0.5 mCi), ^{177}Lu-DOTA-PEG-Cy5-C' dots (1 mCi), ^{177}Lu-DOTA-αMSH-PEG-Cy5-C' dots (0.5 mCi) and ^{177}Lu-DOTA-αMSH-PEG-Cy5-C' dots (1.0 mCi), respectively. The Gehan-Breslow-Wilcoxon test demonstrated statistical difference for the survival data (p=0.029). A survival comparison of individual treatment groups to PBS control showed statistical significance in M21 tumor-bearing mice that received 0.5 mCi of ^{177}Lu-DOTA-αMSH-PEG-Cy5-C' dots (p=0.036) and 1 mCi ^{177}Lu-DOTA-PEG-Cy5-C' dots (p=0.01). There was a significant survival advantage for the mice treated with ^{177}Lu-DOTA- αMSH-PEG-Cy5-C' dots (0.5 mCi) compared to mice treated with 0.5 mCi of non-targeting ^{177}Lu-DOTA-PEG-Cy5-C' dots (p=0.021). Mice that received 1 mCi of ^{177}Lu-DOTA-αMSH-PEG-Cy5-C' dots, 0.5 mCi ^{177}Lu-DOTA-PEG-Cy5-C' dots or non-radiolabeled DOTA-αMSH-PEG-Cy5-C' dots did not exhibit a statistically significant improvement in survival. Non-radiolabeled DOTA-αMSHPEG-Cy5-C' dots were not expected to provide an increase in survival compared to PBS control. The lack of a survival benefit for mice receiving 1 mCi of ^{177}Lu-DOTA-αMSH-PEG-Cy5-C' dots was likely due to its being at the MTD level, resulting in radiotoxicity and removal of mice from the study due to poor body score or weight loss. It is interesting that the mice receiving 1 mCi of non-MC1-R targeted ^{177}Lu-DOTA-PEG-Cy5-C' dots did show a survival benefit without the same degree of radiotoxicity. This is likely due to non-specific enhanced permeability and retention (EPR) effects at the target site, coupled with more rapid renal clearance, mimicking a reduced treatment dose. Cell binding studies with non-targeted ^{177}Lu-DOTA-PEG-Cy5-C' dots showed approximately 38% of the uptake found for targeted ^{177}Lu-DOTA-αMSH-PEG-Cy5-C' dots at 24 h (Fig. S4 and Fig. 3b). This would equate the 1 mCi administered treatment dose to approximately 400 μCi, which is consistent with the therapy results. Blood chemistries showed no signs of hematological toxicities, and were nearly identical for all treatment groups compared to PBS or non-tumor

bearing controls, except for lymphocytes which were slightly lower in the ^{177}Lu-DOTA labeled C' dot groups (Table S3). Average body weights of mice in treatment groups receiving radioactive C' dots were not significantly different from those groups receiving non-radiolabeled C' dots or PBS controls, even though the numbers decreased due to removal of animals for tumor size and poor body score (Fig. S5a).

Treatment efficacy of ^{177}Lu-DOTA-αMSH-PEG-Cy5-C' dots was also examined in B16F10 mice (Fig. 6c and Fig. 6d) receiving subcutaneous flank injections (i.e., 1 million B16F10 cells) 7 days prior to treatment. Mice were randomized according to body weights into treatment groups with equal numbers of male and female mice. The treatment dose was set at 0.5 mCi per mouse based on the results of the M21 therapy study. B16F10 melanoma mice were administered 0.5 mCi ^{177}Lu-DOTA-αMSH-PEG-Cy5-C' dots, 0.5 mCi ^{177}Lu-DOTA-PEG-Cy5-C' dots, DOTA-αMSH-PEG-Cy5-C' dots, or a PBS control via the tail vein. The rate of tumor growth was lower in groups treated with radiotherapeutic C' dots than in groups receiving non-radiolabeled C' dots or PBS over the first 14 days of therapy (Fig. 6c). Kaplan Meier survival analysis yielded median survival times of 16, 14, 21, and 25 days for PBS control, DOTA-PEG-Cy5-C' dots, ^{177}Lu-DOTA-PEG-Cy5-C' dots (0.5 mCi), and ^{177}Lu-DOTA-αMSH-PEG-Cy5-C' dots (0.5 mCi), respectively. Pairwise Gehan-Breslow-Wilcoxon statistical analyses demonstrated a significant survival improvement in mice treated with 0.5 mCi ^{177}Lu-DOTA-αMSH-PEG-Cy5-C' dots compared with those receiving PBS ($p=0.0005$) or non-radiolabeled C' dots $p=0.002$) (Fig. 6d). Likewise, in the B16F10 therapy study, there was a statistically significant difference seen between tumor-bearing mice treated with ^{177}Lu-DOTA-αMSH-PEG-Cy5-C' dots and those treated with the non-targeted ^{177}Lu-DOTA-PEG-Cy5-C' dots ($p=0.045$). Average body weights of mice remaining in the treatment groups that received radioactive C' dots were not significantly different from those receiving non-radiolabeled C' dots or PBS controls (Fig. S5b).

The in vivo therapy studies mirrored in vitro treatment of B16F10 cells with 1 μCi and 5 μCi of ^{177}Lu-DOTA-αMSH-PEG-Cy5-C' dots (Fig S6). The higher treatment dose showed no significant difference in tumor cell death between ^{177}Lu-DOTA-αMSH-PEG-Cy5-C' dots and ^{177}Lu alone, while the lower dose did show a significant treatment advantage at later time points. The higher doses close to MTD resulted in high non-specific toxicities that masked the therapeutic potential of the targeted ^{177}Lu-DOTA-αMSH-PEG-Cy5-C' dots compared to non-targeted ^{177}Lu-DOTA-PEG-Cy5-C' dots in vivo or ^{177}Lu in vitro.

Tumor growth was initially suppressed over the first two-three weeks post treatment in both the B16F10 and M21 therapy studies, however over time tumor growth resumed and eventually resulted in the mice reaching endpoint criteria. Unless 100% of the malignant cells are killed, the tumors will return. There are several particle-based approaches that could be employed to improve therapeutic efficacy. Multiple low doses of ^{177}Lu-DOTA-PEG-Cy5-C' dots over time would likely allow delivery of a cummulative total dose with less normal tissue toxicities. Combination therapy with chemotherapeutic agents conjugated to the C' dot particles via hydrolyzable linkers have been synthesized and could be used in conjunction with radiolabeled C' dots. The particle itself has been shown to induce ferroptosis in tumor cells, but not in normal cells, and could be used in combination with a chemotherapy agent conjugated C' dots or radiolabeled C' dots [44]. Finally, the C' dots

have been shown to activate immune cell components in the tumor microenvironment, which could leverage more effective combination therapies, such as immunotherapy – C' dot radiotherapy [45].

3.6. Therapy study tissue histology

Harvested tumor, liver, and renal tissue specimens were obtained from ^{177}Lu-DOTA-αMSH-PEG-Cy5-C' dot-treated and PBS non-treated control B16F10 tumor bearing mice, H&E stained, and interpreted by a veterinary pathologist (Fig. 7). An analysis of treated and non-treated liver specimens revealed normal hepatic architecture and hepatocellular morphology without evident histopathology. Likewise, an examination of renal tissues revealed normal architecture of the cortex and outer medulla without pathologic findings. No acute renal damage was observed in treated kidneys. A comparison of tumor tissue specimens for treated versus non-treated animals revealed obvious differences. The treated tumors exhibited large areas of tumor necrosis and hemorrhage with intermingled cords of viable neoplastic cells, while non-treated tumors displayed markedly reduced areas of tumor necrosis. These results are consistent with targeted radiotherapy damage to tumor tissues, with relative sparing of major excretory organs (liver and kidney).

A limited histological survey of specific immune cell populations in harvested tumor tissues was also performed at the time of sacrifice using immunohistochemistry. B16F10 tumor tissue samples, obtained from animals treated with ^{177}Lu-DOTA-αMSH-PEG-Cy5-C' dots, DOTA-αMSH-PEG-Cy5-C' dots, and PBS control, were stained for T-cell markers (CD3, CD8) and the murine F4/80 macrophage marker (Fig. S7). There were no statistically significant differences in the relative percentages of macrophages across specimens, noting that melanin was present in macrophages active in tumor cell turnover. Interestingly, increased percentages of CD3+ T cells were found in tumor tissues treated with ^{177}Lu-DOTA-αMSH-PEG-Cy5-C' dots or DOTA-αMSH-PEG-Cy5-C' dots relative to those treated with PBS control, while only specimens treated with ^{177}Lu-DOTA-αMSH-PEG-Cy5-C' dots showed an increased percentage of CD8+ T cells. These findings suggest that both radiolabeled and non-radiolabeled MC1-R targeted C' dots may prime cytotoxic T cells in the tumor microenvironment, offering the potential to synergize with immunotherapy to improve treatment response and outcomes.

4. Conclusion

Fluorescent core-shell silica nanoparticles synthesized in water, *i.e.* C' dots, containing DOTA conjugated MC1-R avid peptides, were radiolabeled with the beta-particle-emitting radionuclide ^{177}Lu and evaluated for their therapeutic properties in melanoma models. DOTA-αMSH-PEG-Cy5-C' dots demonstrated subnanomolar affinity for MC1-R expressing melanoma cells due to the multi-dentate display of αMSH peptides, leading to efficient internalization. The DOTA-αMSH-PEG-Cy5-C' dot particles demonstrated high radiolabeling efficiency and radiochemical stability with ^{177}Lu. *In vivo*, ^{177}Lu-DOTA-αMSH-PEG-Cy5-C' dots exhibited favorable PK and targeted tumor uptake and retention. Tumor localization of 177Lu-DOTA-αMSH-PEG-Cy5-C' dots could be visualized by SPECT imaging and confirmed histologically. Melanoma-bearing mice treated with ^{177}Lu-

DOTA-αMSH-PEG-Cy5-C' dots exhibited prolonged survival over control groups, highlighting the potential of C' dot targeted radiotherapy. The ultrasmall melanoma-avid theranostic silica nanoparticles studied here combine many of the targeting properties of peptides and antibodies with more favorable pharmacokinetic, clearance, and safety profiles. These properties, in turn, can enhance targeted tumor penetration, accumulation, and retention while abrogating dose-limiting toxicity.

Supplementary Material

Refer to Web version on PubMed Central for supplementary material.

Acknowledgements

References

[1]. Hodi FS, O'Day SJ, McDermott DF, Weber RW, Sosman JA, Haanen JB, Gonzalez R, Robert C, Schadendorf D, Hassel JC, Akerley W, van den Eertwegh AJ, Lutzky J, Lorigan P, Vaubel JM, Linette GP, Hogg D, Ottensmeier CH, Lebbe C, Peschel C, Quirt I, Clark JI, Wolchok JD, Weber JS, Tian J, Yellin MJ, Nichol GM, Hoos A, Urba WJ, Improved survival with ipilimumab in patients with metastatic melanoma, N. Engl. J. Med 363 (2010) 711–723. [PubMed: 20525992]

[2]. Robert C, Thomas L, Bondarenko I, O'Day S, Weber J, Garbe C, Lebbe C, Baurain JF, Testori A, Grob JJ, Davidson N, Richards J, Maio M, Hauschild A, Miller WH Jr., Gascon P, Lotem M, Harmankaya K, Ibrahim R, Francis S, Chen TT, Humphrey R, Hoos A, Wolchok JD, Ipilimumab plus dacarbazine for previously untreated metastatic melanoma, N. Engl. J. Med 364 (2011) 2517–2526. [PubMed: 21639810]

[3]. Salama AK, Pharmacotherapies for the Treatment of Metastatic Melanoma. Clinical Medicine Insights, Clin. Med. Insights Oncol 7 (2013) 137–149. [PubMed: 23843723]

[4]. Eroglu Z, Ribas A, Combination therapy with BRAF and MEK inhibitors for melanoma: latest evidence and place in therapy, Ther. Adv. Med. Oncol 8 (2016) 48–56. [PubMed: 26753005]

[5]. Sullivan RJ, Flaherty KT, Resistance to BRAF-targeted therapy in melanoma, Eur. J. Cancer 49 (2013) 1297–1304. [PubMed: 23290787]

[6]. Larkin J, Hodi FS, Wolchok JD, Combined Nivolumab and Ipilimumab or Monotherapy in Untreated Melanoma, N. Engl. J. Med 373 (2015) 1270–1271.

[7]. Hiniker SM, Reddy SA, Maecker HT, Subrahmanyam PB, Rosenberg-Hasson Y, Swetter SM, Saha S, Shura L, Knox SJ, A Prospective Clinical Trial Combining Radiation Therapy With Systemic Immunotherapyin Metastatic Melanoma, Int. J. Radiat .Oncol. Biol. Phys 96 (2016) 578–588. [PubMed: 27681753]

[8]. Postow MA, Callahan MK, Barker CA, Yamada Y, Yuan J, Kitano S, Mu Z, Rasalan T, Adamow M, Ritter E, Sedrak C, Jungbluth AA, Chua R, Yang AS, Roman RA, Rosner S, Benson B, Allison JP, Lesokhin AM, Gnjatic S, Wolchok JD, Immunologic correlates of the abscopal effect in a patient with melanoma, N. Engl. J. Med 366 (2012) 925–931. [PubMed: 22397654]

[9]. Norain A, Dadachova E, Radionuclide Therapy of Melanoma, Semin. Nucl. Med 46 (2016) 250–259. [PubMed: 27067506]

[10]. Mier W, Kratochwil C, Hassel JC, Giesel FL, Beijer B, Babich JW, Friebe M, Eisenhut M, Enk A, Haberkorn U, Radiopharmaceutical therapy of patients with metastasized melanoma with the melanin-binding benzamide ^{131}I-BA52, J. Nucl. Med 55 (2014) 9–14. [PubMed: 24277756]

[11]. Ren G, Miao Z, Liu H, Jiang L, Limpa-Amara N, Mahmood A, Gambhir SS, Cheng Z, Melanin-targeted preclinical PET imaging of melanoma metastasis, J. Nucl. Med 50 (2009) 1692–1699. [PubMed: 19759116]

[12]. Dadachova E, Moadel T, Schweitzer AD, Bryan RA, Zhang T, Mints L, Revskaya E, Huang X, Ortiz G, Nosanchuk JS, Nosanchuk JD, Casadevall A, Radiolabeled melanin-binding peptides are safe and effective in treatment of human pigmented melanoma in a mouse model of disease, Cancer Biother. Radiopharm 21 (2006) 117–129. [PubMed: 16706632]

[13]. Miao Y, Hylarides M, Fisher DR, Shelton T, Moore H, Wester DW, Fritzberg AR, Winkelmann CT, Hoffman T, Quinn TP, Melanoma therapy via peptide-targeted {alpha}-radiation, Clin. Cancer Res 11 (2005) 5616–5621. [PubMed: 16061880]

[14]. Miao Y, Shelton T, Quinn TP, Therapeutic efficacy of a ^{177}Lu-labeled DOTA conjugated alpha-melanocyte-stimulating hormone peptide in a murine melanoma-bearing mouse model, Cancer Biother. Radiopharm 22 (2007) 333–341. [PubMed: 17651039]

[15]. Eberle AN, Rout B, Qi MB, Bigliardi PL, Synthetic Peptide Drugs for Targeting Skin Cancer: Malignant Melanoma and Melanotic Lesions, Curr. Med. Chem 24 (2017) 1797–1826. [PubMed: 28578648]

[16]. Vanderslice P, Biediger RJ, Woodside DG, Brown WS, Khounlo S, Warier ND, Gundlach CWT, Caivano AR, Bornmann WG, Maxwell DS, McIntyre BW, Willerson JT, Dixon RA, A. Small molecule agonist of very late antigen-4 (VLA-4) integrin induces progenitor cell adhesion, J. Biol. Chem 288 (2013) 19414–19428. [PubMed: 23703610]

[17]. Choi J, Beaino W, Fecek RJ, Fabian KPL, Laymon CM, Kurland BF, Storkus WJ, Anderson CJ, Combined VLA-4-Targeted Radionuclide Therapy and Immunotherapy in a Mouse Model of Melanoma, J. Nucl. Med 59 (2018) 1843–1849. [PubMed: 29959213]

[18]. Vegt E, Melis M, Eek A, de Visser M, Brom M, Oyen WJ, Gotthardt M, de Jong M, Boerman OC, Renal uptake of different radiolabelled peptides is mediated by megalin: SPECT and biodistribution studies in megalin-deficient mice, Eur. J. Nucl. Med. Mol. Imaging 38 (2011) 623–632. [PubMed: 21170526]

[19]. Ow H, Larson DR, Srivastava M, Baird BA, Webb WW, Wiesner U, Bright and stable coreshell fluorescent silica nanoparticles, Nano. Lett 5 (2005) 113–117. [PubMed: 15792423]

[20]. Ma K, Mendoza C, Hanson M, Werner-Zwanziger U, Zwanziger J, Wiesner U, Control of Ultrasmall Sub-10 nm Ligand-Functionalized Fluorescent Core–Shell Silica Nanoparticle Growth in Water, Chem. Mater 27 (2015) 4119–4133.

[21]. Burns AA, Vider J, Ow H, Herz E, Penate-Medina O, Baumgart M, Larson SM, Wiesner U, Bradbury M, Fluorescent silica nanoparticles with efficient urinary excretion for nanomedicine, Nano Letters 9 (2009) 442. [PubMed: 19099455]

[22]. Barteau KP, Ma K, Kohle FFK, Gardinier TC, Beaucage PA, Gillilan RE, Wiesner U, Quantitative Measure of the Size Dispersity in Ultrasmall Fluorescent Organic-Inorganic Hybrid Core-Shell Silica Nanoparticles by Small-Angle-X-ray Scattering, Chem Mater. 31 (2019), 643–657. [PubMed: 30886456]

[23]. Benezra M, Penate-Medina O, Zanzonico PB, Schaer D, Ow H, Burns A, DeStanchina E, Longo V, Herz E, Iyer S, Wolchok J, Larson SM, Wiesner U, Bradbury MS, Multimodal silica nanoparticles are effective cancer-targeted probes in a model of human melanoma, J. Clin. Invest 121 (2011) 2768–2780. [PubMed: 21670497]

[24]. Chen F, Ma K, Benezra M, Zhang L, Cheal SM, Phillips E, Yoo B, Pauliah M, Overholtzer M, Zanzonico P, Sequeira S, Gonen M, Quinn T, Wiesner U, Bradbury MS, Cancer-Targeting Ultrasmall Silica Nanoparticles for Clinical Translation: Physicochemical Structure and Biological Property Correlations, Chem. Mater 29 (2017) 8766–8779. [PubMed: 29129959]

[25]. Chen F, Ma K, Zhang L, Madajewski B, Zanzonico P, Sequeira S, Gonen M, Wiesner U, Bradbury MS, Target-or-Clear Zirconium-89 Labeled Silica Nanoparticles for Enhanced Cancer-Directed Uptake in Melanoma: A Comparison of Radiolabeling Strategies, Chem. Mater 29 (2017) 8269–8281. [PubMed: 29123332]

[26]. Phillips E, Penate-Medina O, Zanzonico PB, Carvajal RD, Mohan P, Ye Y, Humm J, Gönen M, Kalaigian H, Schöder H, Strauss HW, Larson SM, Wiesner U, Bradbury MS, 2014 Clinical translation of an ultrasmall inorganic optical-PET imaging nanoparticle probe. Sci. Transl. Med 6

260ra149 https://stm.sciencemag.org/content/6/260/260ra149.long, (DOI: 10.1126/scitranslmed.3009524).

[27]. Chen F, Zhang X, Ma K, Madajewski B, Benezra M, Zhang L, Phillips E, Turker MZ, Gallazzi F, Penate-Medina O, Overholtzer M, Pauliah M, Gonen M, Zanzonico P, Wiesner U, Bradbury MS, Quinn TP, Melanocortin-1 Receptor-Targeting Ultrasmall Silica Nanoparticles for Dual-Modality Human Melanoma Imaging, ACS Appl. Mater. Interfaces 10 (2018) 4379–4393. [PubMed: 29058865]

[28]. Ma K, Zhang D, Cong Y, Wiesner U, Elucidating the mechanism of silica nanoparticle PEGylation processes using fluorescence correlation spectroscopies, Chem. Mater 28 (2016) 1537–1545.

[29]. Larson DR, Ow H, Vishwasrao HD, Heikal AA, Wiesner U, Webb WW, Silica Nanoparticle Architecture Determines Radiative Properties of Encapsulated Chromophores, Chem. Mater 20 (2008) 2677–2684.

[30]. Kohle FFE, Hinckley JA, Wiesner UB, Dye Encapsulation in Fluorescent Core-Shell Silica Nanoparticles as Probed by Fluorescence Correlation Spectroscopy, J. Phys. Chem. C 123 (2019) 9813–9823.

[31]. Stabin MG, Sparks RB, Crowe E, Olinda/Exm: The Second-Generation Personal Computer Software for Internal Dose Assessment in Nuclear Medicine, J. Nucl. Med 46 (2005) 1023–1027. [PubMed: 15937315]

[32]. Kaplan EL, Meier P, Nonparametric estimation from incomplete observations, J. Amer. Statist. Assoc 53 (1958) 457.

[33]. Hazra A, Gogtay N, Biostatistics Series Module 9: Survival Analysis, Indian J. Dermatol 62 (2017) 251–257. [PubMed: 28584366]

[34]. Ma K, Wiesner U, Modular and Orthogonal Post-PEGylation Surface Modifications by Insertion Enabling Penta-functional Ultrasmall Organic-Silica Hybrid Nanoparticles, Chem. Mater 29 (2017) 6840–6855.

[35]. Sawyer TK, Sanfilippo PJ, Hruby VJ, Engel MH, Heward CB, Burnett JB, Hadley ME, 4-Norleucine, 7-D-phenylalanine-alpha-melanocyte-stimulating hormone: A highly potent α-melanotropin with ultralong biological activity, Proc. Natl. Acad. Sci. USA 77 (1980) 5754–5758. [PubMed: 6777774]

[36]. Yang J, Guo H, Miao Y, Technetium-99m-labeled Arg-Gly-Asp-conjugated alpha-melanocyte stimulating hormone hybrid peptides for human melanoma imaging, Nucl. Med. Biol 37 (2010) 873–883. [PubMed: 21055617]

[37]. Guo H, Shenoy N, Gershman BM, Yang J, Sklar LA, Miao Y, Metastatic melanoma imaging with an (111)In-labeled lactam bridge-cyclized alpha-melanocyte-stimulating hormone peptide, Nucl. Med. Biol 36 (2009) 267–276. [PubMed: 19324272]

[38]. Miao Y, Whitener D, Feng W, Owen NK, Chen J, Quinn TP, Evaluation of the human melanoma targeting properties of radiolabeled alpha-melanocyte stimulating hormone peptide analogues, Bioconjug. Chem 14 (2003) 1177–1184. [PubMed: 14624632]

[39]. Yang J, Xu J, Gonzalez R, Lindner T, Kratochwil C, Miao Y, 2018. (68)Ga-DOTA-GGNle-CycMSH(hex) targets the melanocortin-1 receptor for melanoma imaging. Sci. Transl. Med 10 (2018), eaau4445 https://stm.sciencemag.org/content/10/466/eaau4445.short, (DOI:10.1126/scitranslmed.aau4445). [PubMed: 30404861]

[40]. Miao Y, Hoffman TJ, Quinn TP, Tumor-targeting properties of [90]Y- and ^{177}Lu-labeled alpha-melanocyte stimulating hormone peptide analogues in a murine melanoma model, Nucl. Med. Biol 32 (2005) 485–493. [PubMed: 15982579]

[41]. Miao Y, Quinn TP, Alpha-melanocyte stimulating hormone peptide-targeted melanoma imaging, Front. Biosci 12 (2007) 4514–4524. [PubMed: 17485393]

[42]. Miao Y, Quinn TP, Peptide-targeted radionuclide therapy for melanoma, Crit. Rev. Oncol. Hematol 67 (2008) 213–228. [PubMed: 18387816]

[43]. Miao Y, Benwell K, Quinn TP, [99m]Tc- and ^{111}In-labeled alpha-melanocyte-stimulating hormone peptides as imaging probes for primary and pulmonary metastatic melanoma detection, J. Nucl. Med 48 (2007) 73–80. [PubMed: 17204701]

[44]. Kim SE, Zhang L, Ma K, Riegman M, Chen F, Ingold I, Conrad M, Turker MZ, Gao M, Jiang X, Monette S, Pauliah M, Gonen M, Zanzonico P, Quinn T, Wiesner U, Bradbury MB, Overholtzer M, Ultrasmall nanoparticles induce ferroptosis in nutrient-deprived cancer cells and suppress tumour growth, Nat. Nanotechnol 11 (2016) 977–985. [PubMed: 27668796]

[45]. Urbanska AM, Khanin R, Alidori S, Wong S, Mello BP, Almeida BA, Chen F, Ma K, Turker MZ, Korontsvit T, Scheinberg DA, Zanzonico PB, Wiesner U, Bradbury MS, Quinn TP, McDevitt MR, A genomic profile of local immunity in the melanoma microenvironment following treatment with alpha particle-emitting ultrasmall silica nanoparticles, Cancer Biother. Radiopharm In press.

Highlights

- Unique particle surface chemistry yields favorable targeting and pharmacokinetics

- Nanoparticle therapy results in reduced tumor growth and prolonged survival

- Overcomes dose-limiting toxicities associated with existing therapeutics

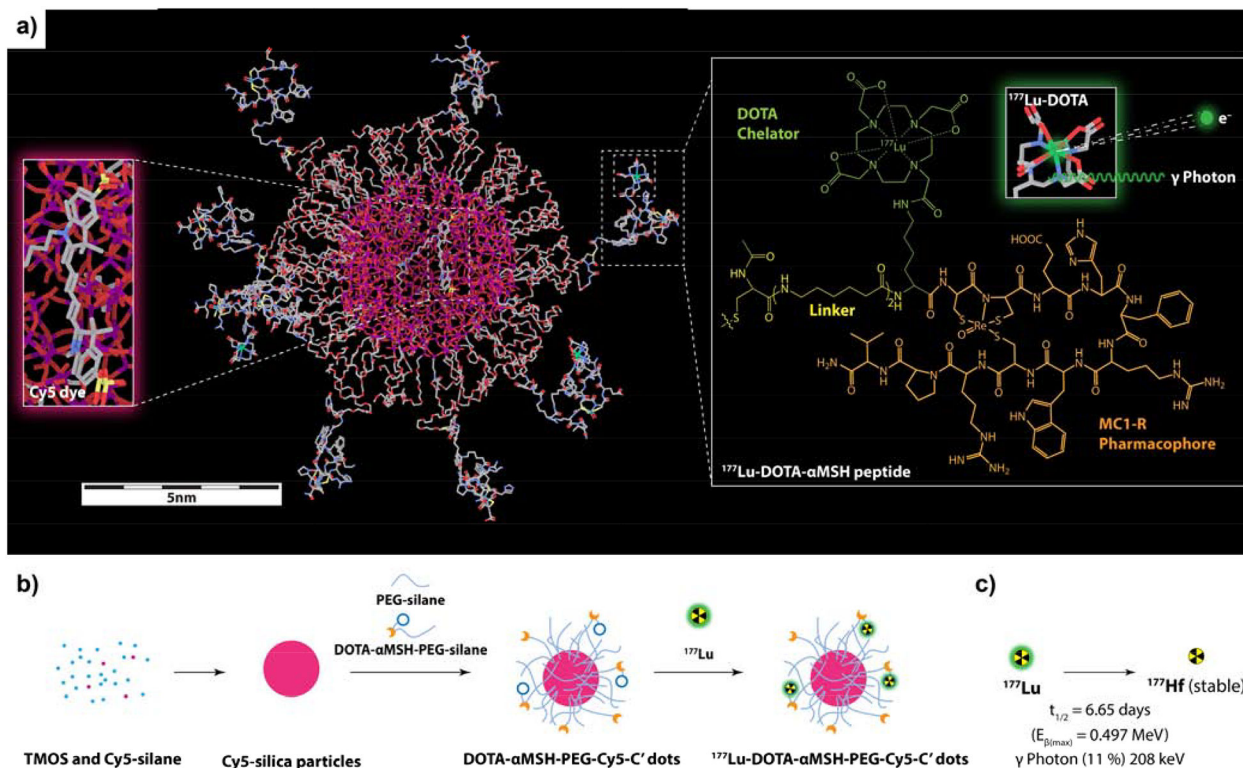- Yields improved treatment efficacy and reduced off-target side effects

Fig. 1.
DOTA-aMSH-PEG-Cy5-C' dots. (a) Molecular rendering of a ^{177}Lu-labeled DOTA-αMSH-PEG-Cy5-C' dot with Cy5 dye-encapsulating silica core (left insert) and the molecular structure of ^{177}Lu-labeled MC1-R targeting cyclic DOTA-αMSH peptides on the right. (b) Schematic of the synthetic approach to DOTA-αMSH-PEG-Cy5-C' dots and its radiolabeling with [177]Lu. (c) Radioactive half-life and decay scheme of predominant beta-emitting particles and imageable gamma photons of [177]Lu.
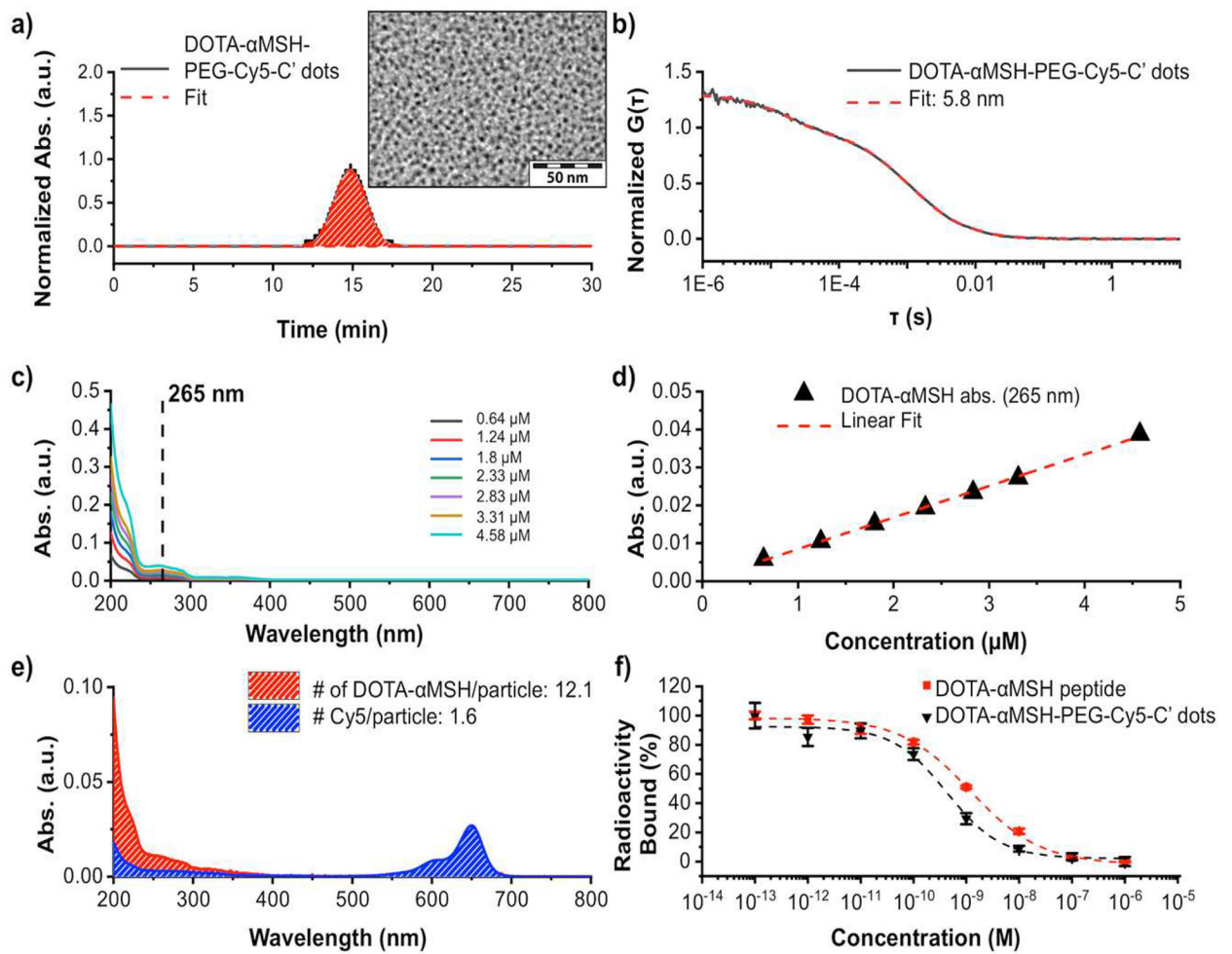
Fig. 2.
DOTA-αMSH-PEG-Cy5-C' dot particle characterization. (a) GPC elugram of purified DOTA-αMSH-PEG-Cy5-C' dots, together with fit using a Gaussian distribution function.[30] (2a-Insert) is a TEM image of particles associated with the GPC peak. (b) DOTA-αMSH-PEG-Cy5-C' dot FCS correlation curve with fit [29–30]. (c,d) DOTA-αMSH peptide absorbance calibration at 265 nm using UV-VIS spectra at various concentrations. (e) Deconvolution of the UV-vis spectrum of DOTA-αMSH-Cy5-C' dot into DOTA-αMSH peptide and PEG-Cy5-C' dot contributions. (f) Competitive binding studies with DOTA-αMSH-PEG-C' dots and DOTA-aMSH peptide with ^{125}I-NDP to B16F10 melanoma cells to determine their IC_{50} values.
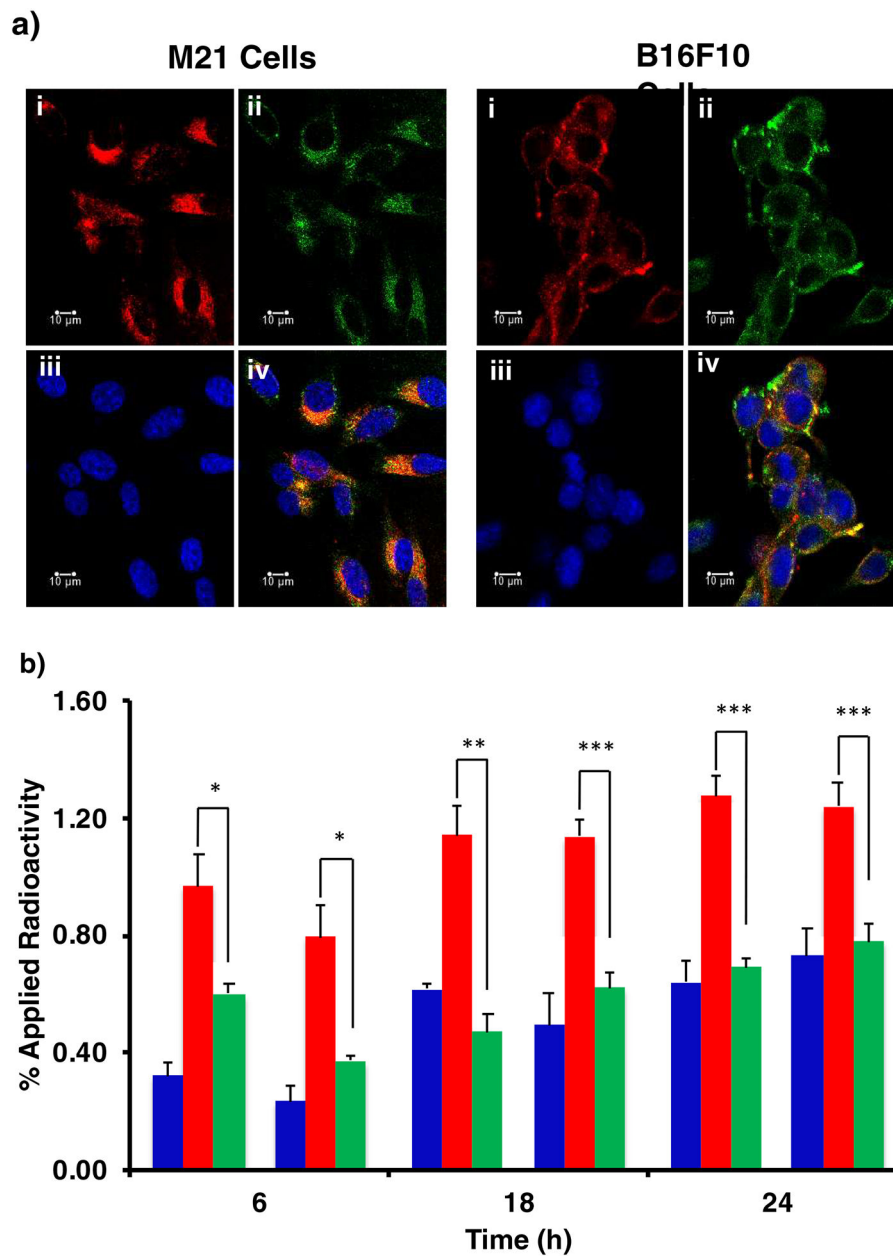
a)

b)

Fig. 3.
(a) Confocal fluorescence microscopy visualization of DOTA-αMSH-PEG-Cy5-C' dots internalization in M21 human melanoma and B16F10 murine melanoma cells at 4 h post administration. M21 and B16F10 melanoma cells were imaged in the presence of DOTA-αMSH-PEG-Cy5-C' dots (i), LysoTracker Green (ii) and Hoechst nuclei stain (iii). Merged images displaying all three probes (iv). Scale bar equals 10 μm. (b) Cell binding and internalization of ^{177}Lu-DOTA-αMSH-PEG-Cy5-C' dots in B16F10 and M21 melanoma cells. Membrane bound (■) and internalized (■) radioactivity were determined at 6 h, 18 h, and 24 h post incubation with ^{177}Lu-DOTA-αMSH-PEG-Cy5-C' dots. Co-incubation of ^{177}Lu-DOTA-αMSH-PEG-Cy5-C' dots with the MC1-R avid NDP blocking peptide (■) was used to assess specificity of internalization. The significance of internalized versus

blocked activity is given as $*p < 0.05$. $**p < 0.01$ and $***p < 0.005$. Each data point represents the mean $\pm$ s.d. of 3 replicates.
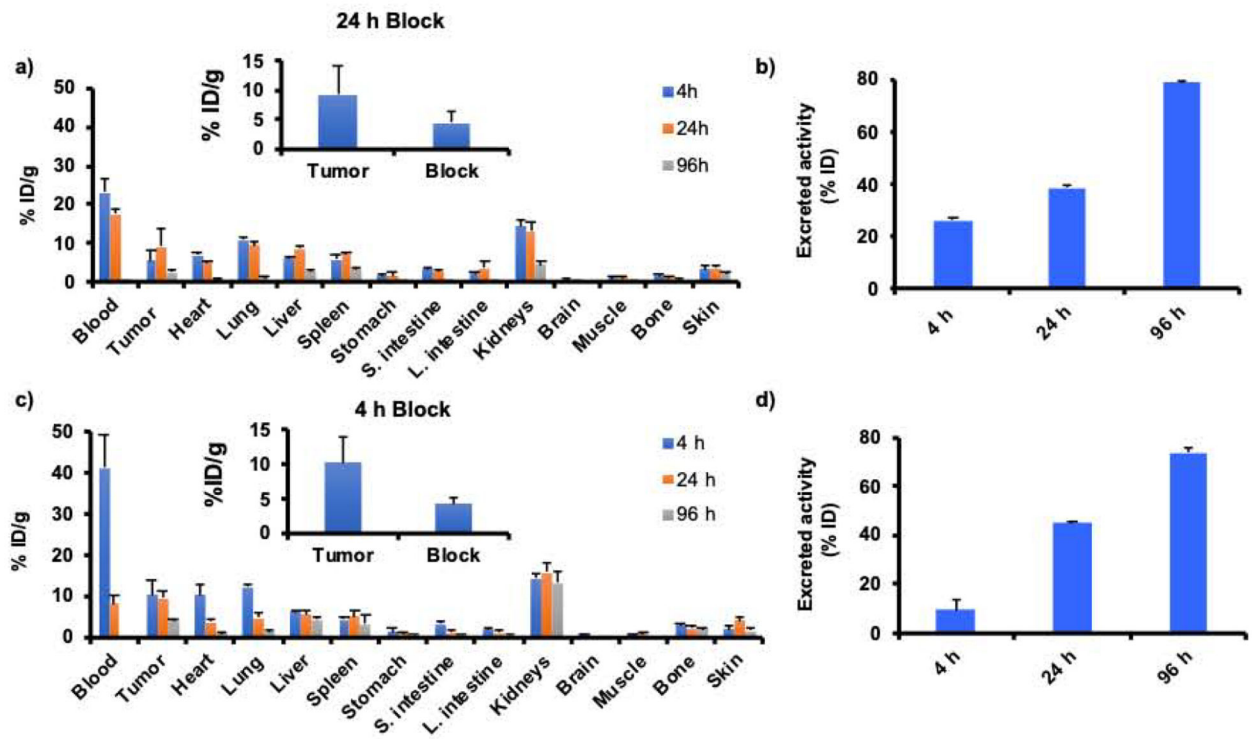
Fig. 4.
Biodistribution of ^{177}Lu-DOTA-αMSH-PEG-Cy5-C' dots in (a-b) M21 and (c-d) B16F10 tumor bearing mice (n=4) at 4 h, 24 h and 96 h post injection reported as injected dose per gram of tissue (% ID/g). Clearance of radioactivity in the urine was reported as percent injected dose (% ID). A blocking study was performed by co-injecting ^{177}Lu-DOTA-αMSH-PEG-Cy5-C' dots + 5μg of NDP (inserts). The blocking study was performed at the time point of maximum ^{177}Lu-DOTA-αMSH-PEG-Cy5-C' dot uptake. Excreted activity is defined as that measured in urine at 4 h and in urine plus feces at 24 h and 96 h.
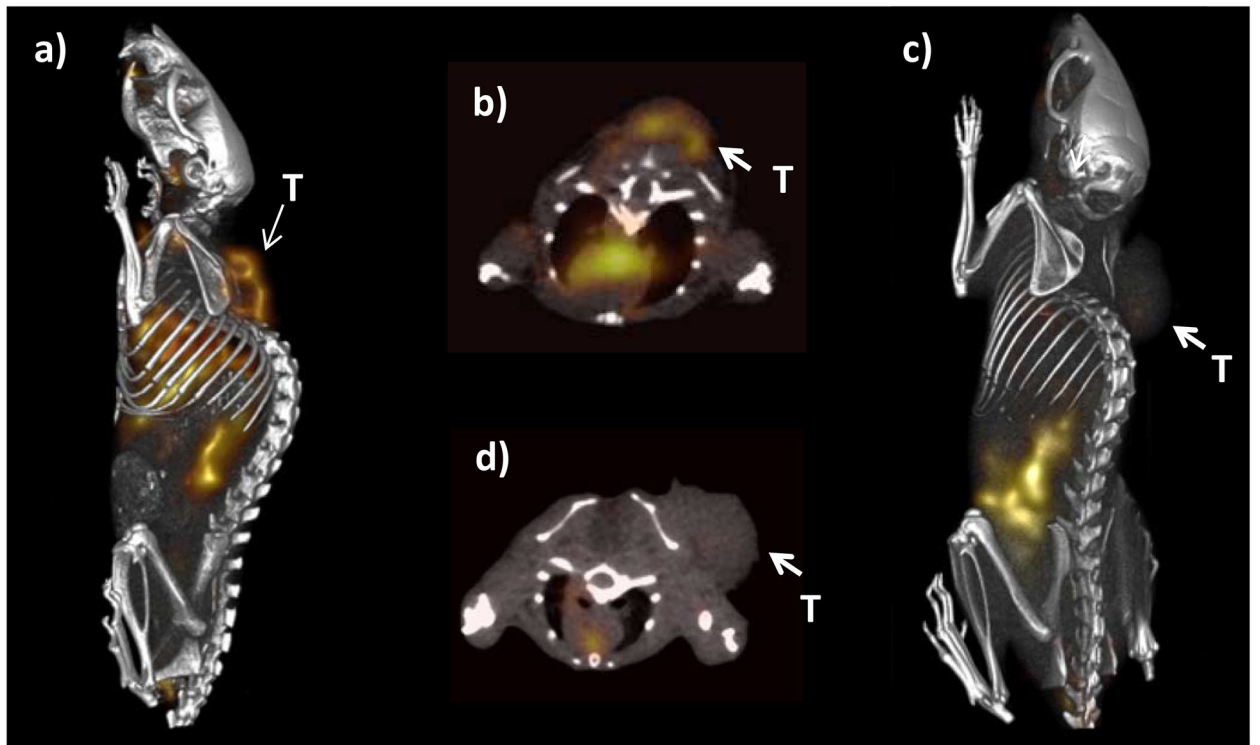
Fig. 5.
^{177}Lu-DOTA-αMSH-PEG-Cy5-C' dot SPECT imaging of M21 melanoma tumor bearing mice at 24 h post injection. (a) Whole body and (b) transaxial images with ^{177}Lu-DOTA-αMSH-PEG-Cy5-C' dots. (c) Whole body and (d) transaxial images showing tumor uptake blocked with ^{177}Lu-DOTA-αMSH-PEG-Cy5-C' dots + NDP peptide (T = Tumor).
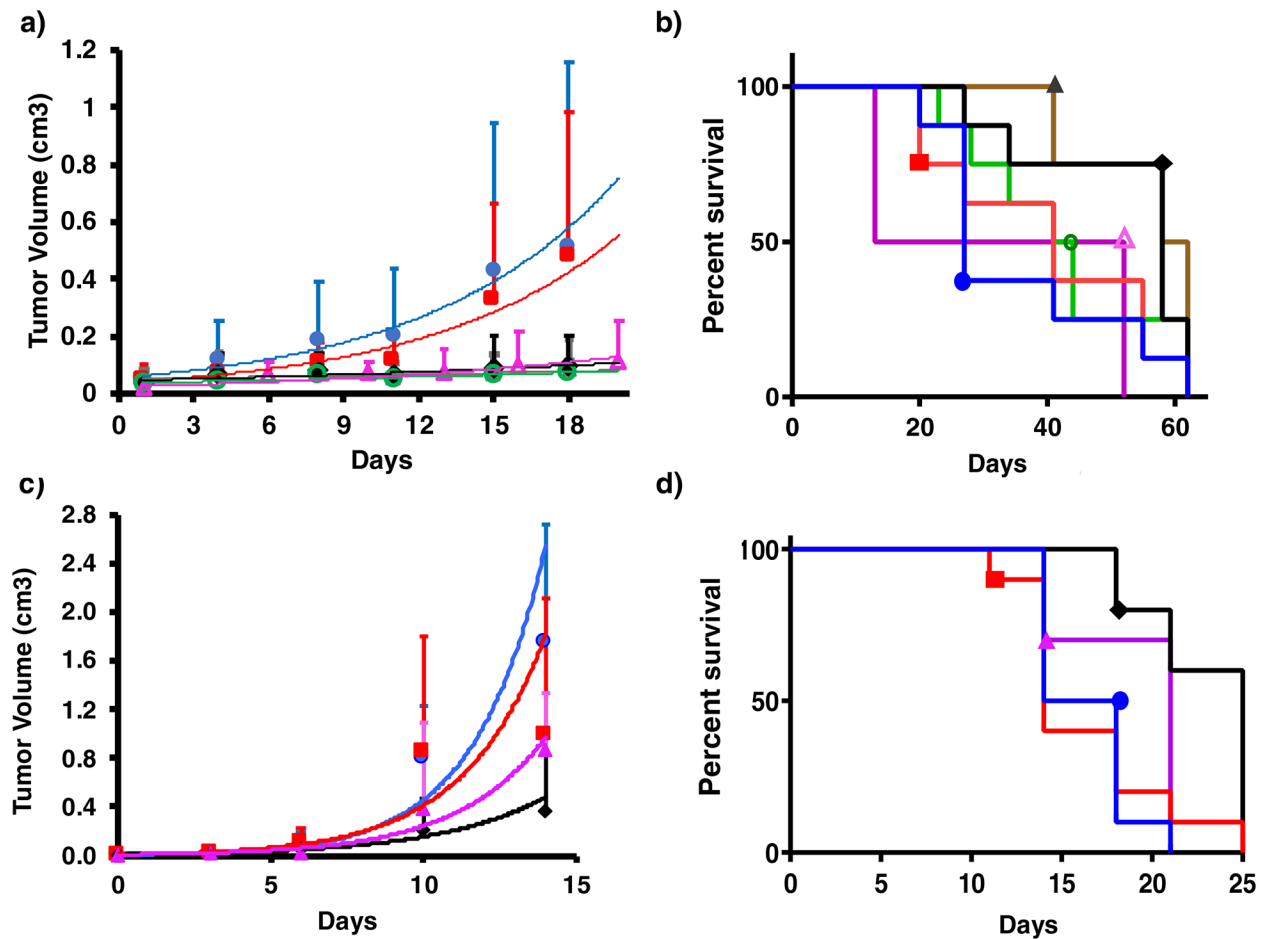
Fig. 6.

Tumor volume and survival plots for M21 and B16F10 melanoma-bearing mice treated with ^{177}Lu-DOTA-αMSH-PEG-Cy5-C' dots. Tumor growth rate plots for (a) M21 xenografted mice and (b) Kaplan-Meier survival plots. M21 tumor mice were administered 1 mCi ^{177}Lu-DOTA-αMSH-PEG-Cy5-C' dots (○), 0.5 mCi ^{177}Lu-DOTA-αMSH-PEG-Cy5-C' dots (◆), 1 mCi ^{177}Lu-DOTA-PEG-Cy5-C' dots (▲), 0.5 mCi ^{177}Lu-DOTA-PEG-Cy5-C' dots ( ), DOTA-αMSH-PEG-Cy5-C' dots (■), or PBS (●). (c) B16F10 mice tumor growth rates and (d) Kaplan-Meier survival plots. B16F10 tumor mice were administered 0.5 mCi ^{177}Lu-DOTA-αMSH-PEG-Cy5-C' dots (◆), 0.5 mCi ^{177}Lu-DOTA-PEG-Cy5-C' dots (▲), DOTA-αMSH-PEG-Cy5-C' dots (■), or PBS (●). M21 tumor bearing mice receiving 0.5 mCi of ^{177}Lu-DOTA-αMSH-PEG-Cy5-C' dots exhibited significantly improved survival compared to the PBS group *(p=0.036) and mice receiving 0.5 mCi ^{177}Lu-DOTA-PEG-Cy5-C' dots *(p=0.021). Mice receiving 1 mCi of the non-targeted ^{177}Lu-DOTA-PEG-Cy5-C' dots also demonstrated a survival advantage *(p=0.01), while the 1 mCi ^{177}Lu-DOTA-αMSH-PEG-Cy5-C' dots treated group did not. B16F10 tumor bearing mice receiving 0.5 mCi of ^{177}Lu-DOTA-αMSH-PEG-Cy5-C' dots demonstrated a significant survival improvement compared to mice receiving PBS ***(p=0.0005) or non-radiolabeled DOTA-αMSH-PEG-Cy5-C' dots **(p=0.002). There was a significant enhancement in survival for

tumor bearing mice treated with ^{177}Lu-DOTA-αMSH-PEG-Cy5-C' dots versus non-targeted ^{177}Lu-DOTA-PEG-Cy5-C' dots *(p=0.045).
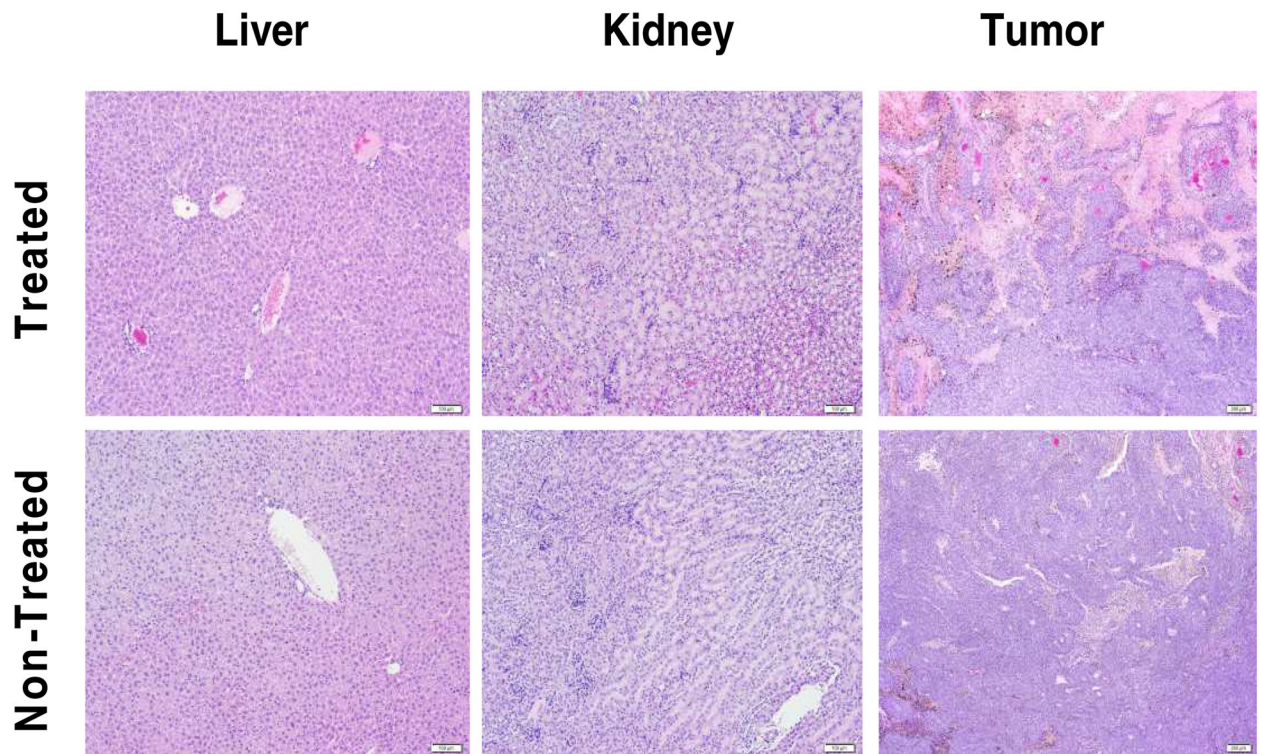
Fig. 7.
Therapy study tissue histopathology. H&E stained liver, kidney and tumor tissue from mice treated with 0.5 mCi ^{177}Lu-DOTA-αMSH-PEG-Cy5-C' dots (upper panels) or non-treated PBS controls (lower panels). Scale bar 100 μm.

Table 1.

Radiation dosimetry for ^{177}Lu-DOTA-αMSH-PEG-Cy5-C' dots in a 70-kg standard human.

Tissue	rad/mci
Adrenals	0.029
Blood	
Brain	0.024
Breasts	0.007
Gallbladder Wall	0.032
Lower Large Intestine Wall	0.191
Small Intestine	0.217
Stomach Wall	0.068
Upper Large Intestine Wall	0.128
Heart Wall	0.211
Kidneys	3.78
Liver	0.877
Lungs	0.493
Muscle	0.201
Ovaries	0.015
Pancreas	0.246
Red Marrow	0.122
Bone	0.787
Spleen	0.751
Testes	0.007
Thymus	0.012
Thyroid	0.009
Uterus	0.013
Total Body	0.150